ISSN (Print) 1226-1750
ISSN (Online) 2233-6656
Journal of Magnetics 25(1), 92-100 (2020) https://doi.org/10.4283/JMAG.2020.25.1.092

Mutual Inductance Analysis of Rectangular Spiral Coils with Angle and Position Variations for Wireless Power Transfer

Juwan Kim[1], Wei Huang[2], Jae Woo Chung[3], and Hyunchul Ku[1]*

[1]*Dept. of Electronic and Comm. Eng., Konkuk University, Seoul 05029, Republic of Korea*
[2]*Transcom Instrument Co. Ltd, Shanghai, China*
[3]*Dept. of Information Comm, Materials and Chemistry Convergence Tech., Soongsil University, Seoul 06978, Republic of Korea*

(Received 3 September 2019, Received in final form 23 March 2020, Accepted 24 March 2020)

For wireless charging, a misalignment between a receiver (Rx) coil in the devices (EV, drone and IMD) and a transmitter (Tx) coil often occurs. In this case, a mutual inductance between the coils changes, and consequently a power transfer efficiency (PTE) of the wireless power transfer (WPT) system also changes. To analyze the WPT system in such a situation, this paper presents an analytical method using Neumann formula to derive mutual inductance considering angular and position variations of two rectangular spiral coils. To verify the proposed method, magnetic resonant WPT systems of 85 kHz and 6.78 MHz are implemented, and the PTE values derived from the analyzed mutual inductance and the measured S-parameters are compared for the cases of angle and position variations. For each case, the two PTE values agree well with each other, and it is verified using the normalized root mean square error (NRMSE) values.

Keywords : Wireless Power Transfer (WPT), mutual inductance, neumann formula

1. Introduction

Wireless power transfer (WPT) has great potential in many applications such as mobile robots, smart phones, non-contact electric vehicle (EV) [1-3], drone and implantable medical devices (IMD). Especially, the magnetic resonant WPT technique which can transmit power at a relatively long distance has actively studied as a method for wireless charging EV, drone and IMD [4-8]. Wireless charging of EV, drone and IMD provides a lot of convenience by eliminating the wires, but depending on the position of the devices, the position change between the transmitter (Tx) coil and the receiver (Rx) coil of the WPT system often occurs. In the magnetic resonant WPT technique, critical coupling occurs when the Tx coil and the Rx coil are aligned in a specific position (generally, when the center axis are the same), and the power transfer efficiency (PTE) is maximized. If there is misalignment between coils from the aligned position, the PTE generally decreases significantly.

The most important factor determining the PTE of the WPT system is the mutual inductance value between the Tx and Rx coils, which depends on the relative position of the coils [9-11]. Therefore, studies have been made on analyzing the characteristics of magnetic resonant coils in many WPT systems. Planar rectangular spiral coils are often used in various applications because they are thin and have relatively high inductance value in small areas [12-14]. Greenhouse analyzed the self and mutual inductance of a planar coil [15]. Many studies have been executed to analyze self and mutual inductance of rectangular coils [12-16]. The inductance analysis using Neumann formula is often utilized in WPT system research [17, 18]. However, few studies have been conducted on the induction of mutual inductance applied to WPT analysis considering the changes in the angle and position of the coils. This is because it is much more complicated than extracting the mutual inductance between aligned coils.

In this paper, we propose a method to calculate the mutual inductance between two rectangular spiral coils. The proposed method converts the spiral coil into a set of rectangular coils of different sizes and calculates the mutual inductance by superposing the Neumann formula considering the changes in the angle and position of the Rx coil. As a result, closed-form equations of mutual inductance, expressed as a function of angle difference

*Corresponding author: Tel: +82-2-2049-6118
Fax: +82-2-3437-5235, e-mail: hcku@konkuk.ac.kr

and horizontal position difference, can be derived respectively. The extracted mutual inductances are utilized for PTE analysis of the magnetic resonant WPT system. The PTE is simulated using the obtained mutual inductance and the equivalent circuit model of the WPT system. In addition, the calculated mutual inductance is used to determine the optimal position of the Rx coil for maximizing the PTE. For experimental verification, 85 kHz (the standard frequency of EV) and 6.78 MHz (the standard frequency of drone and IMD) magnetic resonant WPT systems with rectangular spiral coils are implemented respectively, and the PTE values are measured with S-parameters by changing the angle and position of the Rx coil. The accuracy of the proposed method is verified by comparing the predicted and measured values for the PTE of the WPT systems.

2. Mutual Inductance for Rectangular Spiral Coils

Figure 1(a) shows a rectangular spiral coil. The width and length of the outermost layer of the coil are 2α and 2β, respectively. To calculate a mutual inductance between multi-turn coils, the coil is approximated by a set of concentric single-turn rectangular coils, as shown in Fig. 1(b). We set the outermost rectangular coil as the first layer and the second outermost one as the second layer so on. Accordingly, the innermost layer becomes the *N-th* layer of the N turned spiral coil. If the distance between the adjacent turns of the spiral coil is d, the width and length of the second layer of the coil are $2(\alpha–d)$ and $2(\beta–d)$, respectively. In order to obtain the mutual inductance of the case where the centers are on the same axis and there is no angular rotation between the two rectangular coils (this case is denoted as aligned in this paper), we consider the configuration shown in Fig. 2.

The centers of the Tx and Rx coils are $O_1(0, 0, 0)$ and $O_2(0, 0, h)$; the turn intervals and the number of turns for

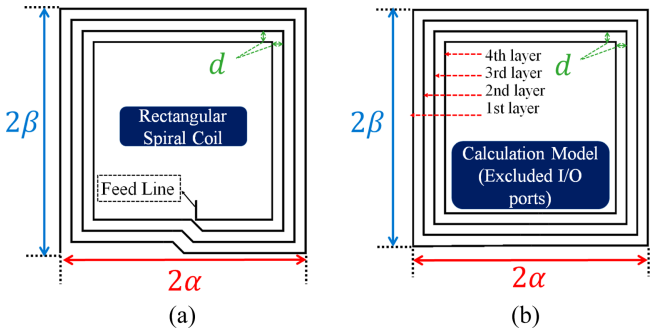

Fig. 1. (Color online) (a) Multi-turn rectangular spiral coil, (b) Set of single-turn rectangular coil.

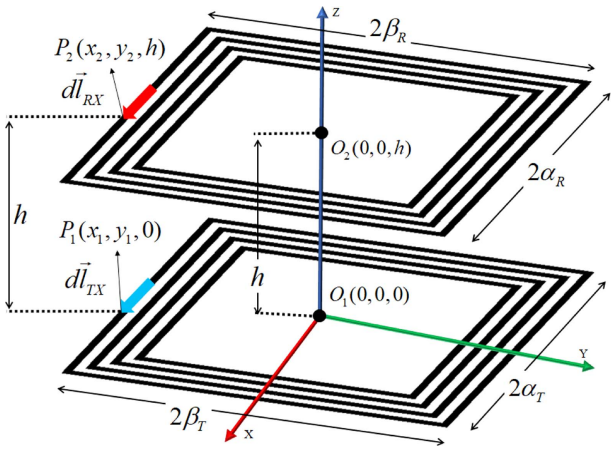

Fig. 2. (Color online) Configuration of center-aligned rectangular spiral coils without angle variation.

Tx and Rx coils are, d_1, d_2 and N_T, N_R; The widths and lengths of the outermost layers of two coils are $2\alpha_T$, $2\beta_T$ and $2\alpha_R$, $2\beta_R$, respectively. The locations of the Tx and Rx coils are $P_1(x_1, y_1, 0)$ and $P_2(x_2, y_2, h)$ as shown in Fig. 2. The total mutual inductance (M_{total}) between the multi-turn coils can be obtained as follows:

$$M_{total} = \sum_{m=1}^{N_T} \sum_{n=1}^{N_R} M_{mn} \tag{1}$$

where M_{mn} is the mutual inductance between the two

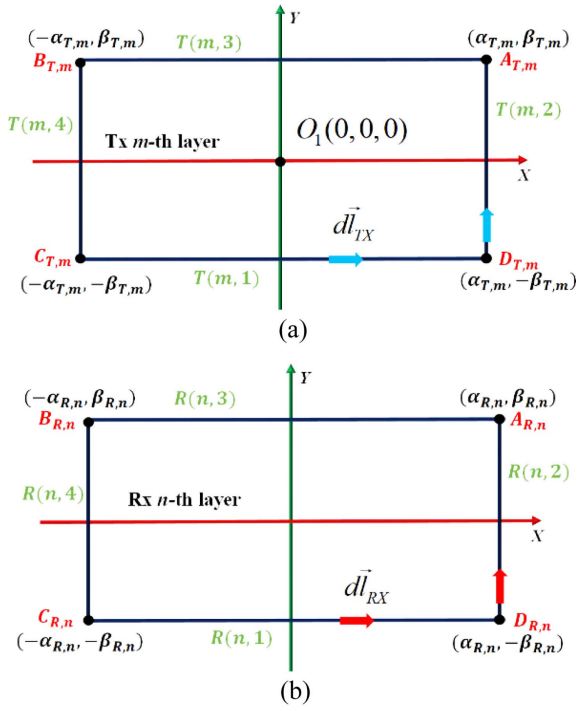

Fig. 3. (Color online) Segmentation of rectangular coil. (a) *m*-th layer of the Tx coil, (b) *n*-th layer of the Rx coil.

single-turn coils (*m*-th Tx coil and *n*-th Rx coil, $m = 1, ..., N_T$, $n = 1, ..., N_R$). In addition, a layer is divided into four segments, and their mutual inductances are calculated. The four sides of the *m*-th layer of the Tx coil and those of the *n*-th layer of the Rx coil are represented by $T(m,i)$ and $R(n,j)$ respectively as shown in Fig. 3, $i = 1,...,4$ and $j = 1,...,4$. Here, *i* and *j* represent the four sides of the Tx and Rx coils. $A_{(T,m)}, B_{(T,m)}, C_{(T,m)}$ and $D_{(T,m)}$ represent the four vertices of a rectangle in the *m*-th layer of the Tx coil. $A_{(R,n)}, B_{(R,n)}, C_{(R,n)}$ and $D_{(R,n)}$ represent the four vertices of a rectangle in the *n*-th layer of the Rx coil. In Fig. 3, $\alpha_{(T,m)} = \alpha_T - (m-1)d_1$, $\beta_{(T,m)} = \beta_T - (m-1)d_1$, $\alpha_{(R,n)} = \alpha_R - (n-1)d_2$ and $\beta_{(R,n)} = \beta_R - (n-1)d_2$.

The length of the $T(m,i)$ is $2\alpha_{(T,m)}(i = 1,3)$ and $2\beta_{(T,m)}(i = 2, 4)$, and the length of the $R(n,j)$ is $2\alpha_{(R,n)}(j = 1,3)$ and $2\beta_{(R,n)}(j = 2,4)$. M_{mn} in Eq. (1) can be obtained as follows.

$$M_{mn} = \sum_{i}^{4}\sum_{j}^{4} M_{T(m,i),R(n,j)} \tag{2}$$

where $M_{T(m,i),R(n,j)}$ is the mutual inductance between the elements of coils $T(m,i)$ and $R(n,j)$. The following Neumann formula [15, 19] is used to calculate M_{mn}:

$$M_{mn} = \frac{\mu_0}{4\pi}\oint_{TX}\oint_{RX}\frac{d\overrightarrow{l_{TX}} \bullet d\overrightarrow{l_{RX}}}{R} \tag{3}$$

where $\mu_0$is the magnetic permeability of free space. The vectors $d\overrightarrow{l_{TX}}$ and $d\overrightarrow{l_{RX}}$ in Fig. 3 are expressed in the Cartesian coordinate system as follows:

$$d\overrightarrow{l_{TX}} = \begin{cases} dx_1\vec{x} & i = 1 \\ dy_1\vec{y} & i = 2 \\ -dx_1\vec{x} & i = 3 \\ -dy_1\vec{y} & i = 4 \end{cases} \quad d\overrightarrow{l_{RX}} = \begin{cases} dx_2\vec{x} & j = 1 \\ dy_2\vec{y} & j = 2 \\ -dx_2\vec{x} & j = 3 \\ -dy_2\vec{y} & j = 4 \end{cases} \tag{4}$$

where $\vec{x}$ and $\vec{y}$ are unit vectors in the 3-dimensional Cartesian coordinates shown in Fig. 3. *R* is the distance between P_1 and P_2 in Fig. 2, and it is as follows:

$$R = \sqrt{(x_2 - x_1)^2 + (y_2 - y_1)^2 + h^2} \tag{5}$$

The mutual inductance between *T*(*m*, 1) and *R*(*n*, *j*) can be obtained using Eq. (3), Eq. (4), and Eq. (5) as follows:

$$M_{T(m,1),R(n,1)} = \frac{\mu_0}{4\pi}\int_{-\alpha_{R.n}}^{\alpha_{R.n}}\int_{-\alpha_{T,m}}^{\alpha_{T,m}}\frac{dx_1 dx_2}{R_1} \tag{6}$$

$$R_1 = \sqrt{(x_2 - x_1)^2 + (\beta_{T,m} - \beta_{R,n})^2 + h^2} \tag{7}$$

$$M_{T(m,1),R(n,3)} = \frac{\mu_0}{4\pi}\int_{-\alpha_{R.n}}^{\alpha_{R.n}}\int_{-\alpha_{T,m}}^{\alpha_{T,m}}\frac{-dx_1 dx_2}{R_2} \tag{8}$$

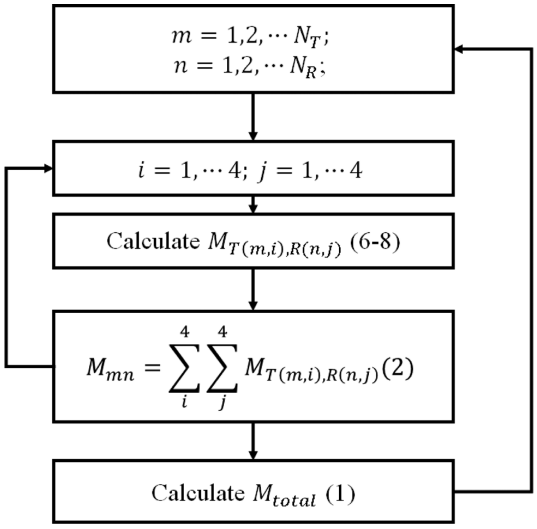

Fig. 4. Flow chart for calculating mutual inductance.

$$R_2 = \sqrt{(x_2 - x_1)^2 + (\beta_{T,m} + \beta_{R,n})^2 + h^2} \tag{9}$$

$$M_{T(m,1),R(n,2)} = M_{T(m,1),R(n,4)} = 0 \tag{10}$$

Similarly, the mutual inductances between the other *T*(*m*, *i*) and *R*(*n*, *j*) can be calculated. The mutual inductance value between the components perpendicular to each other becomes zero as shown in Eq. (10).

By adding these values, we can get M_{mn} and finally M_{total}. Fig. 4 shows the overall procedure of obtaining the mutual inductance.

3. Mutual Inductance of Position and Angular Variations

In this section, we analyze the mutual inductance considering the variations in the angle and position of the Rx coil. Fig. 5 shows examples of WPT charging systems for EV and drone. Typical frequency specifications used in each case are 85 kHz and 6.78 MHz, respectively. As shown in Fig. 5, the Tx and Rx coils may be aligned at the desired position or may be misaligned. In the case of misalignment, the change in angle or position between coils often occurs as shown in Fig. 5.

Figure 6(a) shows a case where the Rx coil is rotated by the angle θ compared to the case where the Rx coil is aligned. Fig. 6(b) shows the shape of the rotated *n*-th layer rectangle of the Rx coil and its coordinate values. For the angular variation case *T*(*m*, *i*) and *R*(*n*, *j*) (*j* = 2, 4) are no longer perpendicular to each other. Therefore, the four sides of the Rx coil will affect the four sides of the Tx coil. The rotated vertex of $A_{(R,n)}(\alpha_{(R,n)}, \beta_{(R,n)})$ is denoted as $A'_{(R,n)}$, which is $(A'_{(R,n\_x)}, A'_{(R,n\_y)})$ in the *x*-*y* plane. Then $A'_{(R,n)}$ can be expressed by multiplying

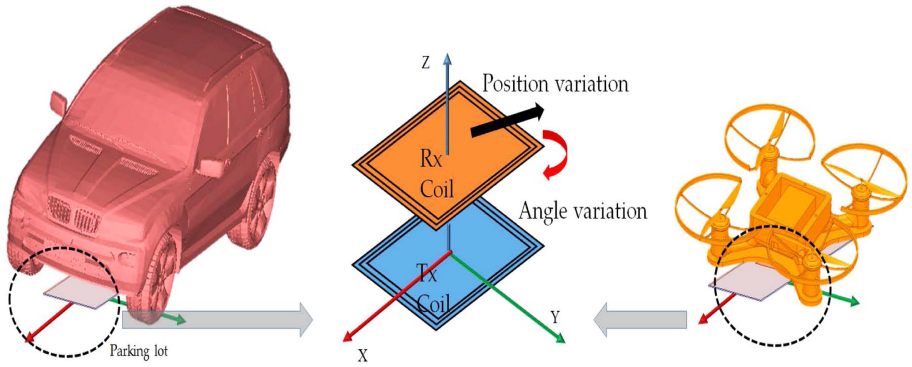

Fig. 5. (Color online) Example of coil misalignment in wireless charging of EV and drone.

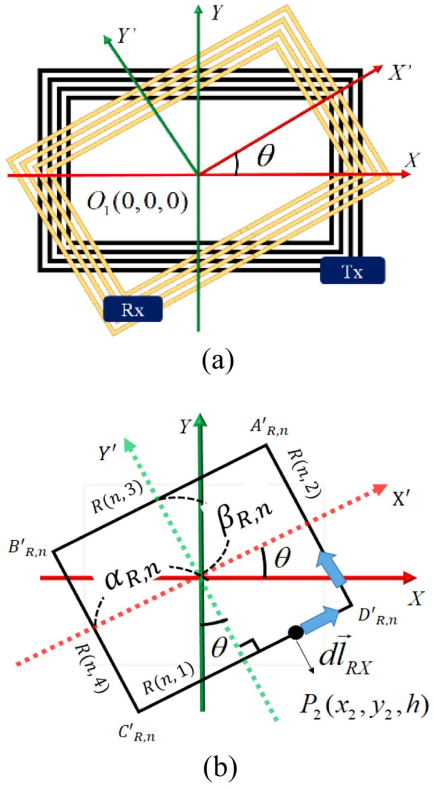

Fig. 6. (Color online) View of the Tx and Rx coils in x-y domain considering angle rotation, (a) top view of the coil, (b) top view of the *n*-th layer of Rx coil and its coordinate.

the vertex of $A_{(R,n)}$ in Fig. 3 by the rotation matrix as follows:

$$\begin{bmatrix} A'_{R,n\_x} \\ A'_{R,n\_y} \end{bmatrix} = \begin{bmatrix} \cos\theta & -\sin\theta \\ \sin\theta & \cos\theta \end{bmatrix} \begin{bmatrix} \alpha_{R,n} \\ \beta_{R,n} \end{bmatrix} \tag{11}$$

In the same way, the coordinate values of the other three rotated vertices, $B'_{R,n}(B_{R,n\_x}, B_{R,n\_y})$, $C'_{R,n}(C_{R,n\_x}, C_{R,n\_y})$, $D'_{R,n}(D_{R,n\_x}, D_{R,n\_y})$ can be obtained. For this case, Eq. (6) and Eq. (10) can be rewritten as follows by considering the angular rotation:

$$M_{T(m,1),R(n,1)}(\theta) = \frac{\mu_0}{4\pi} \int_{C'_{R,n\_x}}^{D'_{R,n\_x}} \int_{-\alpha_{T,m}}^{\alpha_{T,m}} \frac{dx_1 dx_2}{R_3} \tag{12}$$

$$R_3 = \sqrt{(x_2 - x_1)^2 + (x_2 \tan\theta - \frac{\beta_{R,n}}{\cos\theta} + \beta_{T,m})^2 + h^2} \tag{13}$$

$$C'_{R,n\_x} = -\alpha_{R,n}\cos\theta + \beta_{R,n}\sin\theta \tag{14}$$

$$D'_{R,n\_x} = \alpha_{R,n}\cos\theta + \beta_{R,n}\sin\theta \tag{15}$$

$$M_{T(m,1),R(n,2)}(\theta) = \frac{\mu_0}{4\pi} \int_{A'_{R,n\_x}}^{D'_{R,n\_x}} \int_{-\alpha_{T,m}}^{\alpha_{T,m}} \frac{-dx_1 dx_2}{R_4} \tag{16}$$

$$R_4 = \sqrt{(x_2 - x_1)^2 + (-\frac{x_2}{\tan\theta} + \frac{\alpha_{R,n}}{\sin\theta} + \beta_{T,m})^2 + h^2} \tag{17}$$

$M_{(T(m,i),R(n,j))}(\theta)(j = 3,4)$ can be extracted in the similar way. All $M_{(T(m,i),R(n,j))}$ is a function of θ, and we can extract overall mutual inductance between two rectangular spiral coils by superposing these equations. For the angular variation, we can extract $M_{total}(\theta)$ which is a function of θ.

Figure 7(a) shows a case where the Rx coil is horizontally moved by Δx and Δy in the x and y directions, respectively. Fig. 7(b) shows the shape of the n-th layer rectangle of the Rx coil and its coordinate values.

For the position variation case shown in Fig. 7, the Eq. (6-9) can be rewritten as follows by considering the lateral position change.

$$M_{T(m,1),R(n,1)}(\Delta x, \Delta y) = \frac{\mu_0}{4\pi} \int_{-\alpha_{R,n}+\Delta x}^{\alpha_{R,n}+\Delta x} \int_{-\alpha_{T,m}}^{\alpha_{T,m}} \frac{dx_1 dx_2}{R_5} \tag{18}$$

$$R_5 = \sqrt{(x_2 - x_1)^2 + (\beta_{T,m} - \beta_{R,n} + \Delta y)^2 + h^2} \tag{19}$$

$$M_{T(m,1),R(n,3)}(\Delta x, \Delta y) = \frac{\mu_0}{4\pi} \int_{-\alpha_{R,n}+\Delta x}^{\alpha_{R,n}+\Delta x} \int_{-\alpha_{T,m}}^{\alpha_{T,m}} \frac{-dx_1 dx_2}{R_6} \tag{20}$$

$$R_6 = \sqrt{(x_2 - x_1)^2 + (\beta_{T,m} + \beta_{R,n} + \Delta y)^2 + h^2} \tag{21}$$

For the lateral movement case, the mutual inductance value between the components perpendicular to each other becomes zero as follows:

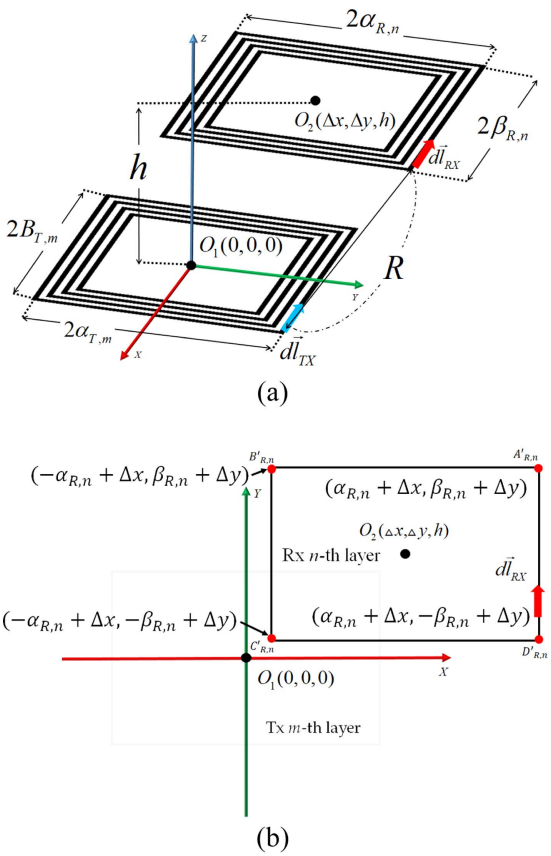

Fig. 7. (Color online) View of WPT system with lateral movement of Rx coil, (a) 3D view, (b) top view of the n-th layer of Rx coil and its coordinate.

$$M_{T(m,1),R(n,2)} = M_{T(m,1),R(n,4)} = 0 \tag{22}$$

Using the procedure in Fig. 4, we can finally derive $M_{total}(\Delta x,\Delta y)$, which is a function of lateral variation.

4. Analysis of WPT using Mutual Inductance

Figure 8 shows a circuit diagram of a magnetic resonant coupling WPT system with series capacitors.

L_{TX} and L_{RX} are self-inductance of the Tx and Rx coils, respectively. M is the mutual inductance between the two coils. The capacitance of the Tx and Rx WPT systems are represented by C_1 and C_2, respectively. The theoretical values can be extracted using $\omega_0 = 1/\sqrt{L_{TX}C_1} = 1/\sqrt{L_{RX}C_2}$, where $\omega_0 (= 2\pi f_0)$ is the resonant angular frequency of the WPT system. V is the phasor of the voltage source of the Tx coil. R_1 and R_2 denote the parasitic resistances of the two coils, respectively. R_S is the source resistance, and R_L is the load resistance. The PTE from the Tx coil to the Rx coil, i.e., η_{21}, can be calculated using the S-parameter S_{21} as follows [19]:

$$\eta_{21} = |S_{21}|^2 \times 100\% \tag{23}$$

S_{21} for WPT system, shown in Fig. 8, can be obtained as follows [20]:

$$S_{21} = \frac{2Z_{21}\sqrt{R_S R_L}}{(Z_{11}+R_S)(Z_{22}+R_L)-Z_{12}Z_{21}} \tag{24}$$

$$Z_{11} = R_1 + j\omega L_{TX} + \frac{1}{j\omega C_1} \tag{25}$$

$$Z_{22} = R_2 + j\omega L_{RX} + \frac{1}{j\omega C_2} \tag{26}$$

$$Z_{12} = Z_{21} = j\omega M \tag{27}$$

Eq. (24) can be rewritten as a function of mutual inductance as in Eq (28):

$$S_{21} = \frac{2j\omega M\sqrt{R_S R_L}}{\omega^2 M^2 + (Z_{11}+R_S)(Z_{22}+R_L)} \tag{28}$$

The mutual inductance that maximizes η_{21} at the resonant frequency ω_0 can be obtained by determining the mutual inductance that satisfies the relationship, $\partial|S_{21}|/\partial M = 0$, as follows:

$$M = \sqrt{(R_1+R_S)(R_2+R_L)/\omega_0^2} \tag{29}$$

The angle and position of the Rx coil where the PTE becomes maximum can be obtained by comparing the mutual inductance obtained in the previous section with that obtained using Eq. (29).

5. Simulated and Experimental Results

To validate the proposed mutual inductance calculation

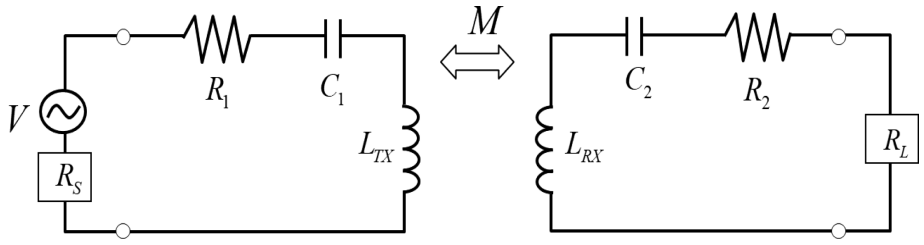

Fig. 8. Circuit diagram of WPT system.

Table 1. Parameters of the WPT system in Case 1 and Case 2.

Note	Symbol	Value	
		Case 1	Case 2
Resonant frequency	f_0	85 kHz	6.78 MHz
Inductance of Tx, Rx	L_{TX}, L_{RX}	131 μH, 13 μH	8.39 μH, 8.42 μH
Half-width of outermost layer	α_T, α_R	225 mm, 125 mm	100 mm, 100 mm
Half-length of outermost layer	β_T, β_R	225 mm, 125 mm	100 mm, 100 mm
Parasitic resistance of Tx, Rx	R_1, R_2	1 Ω, 0.4 Ω	0.52 Ω, 0.56 Ω
Capacitance of Tx, Rx	C_1, C_2	31 nF, 282 nF	56 pF, 58 pF
Resistance of load, source	R_L, R_S	50 Ω	50 Ω
Number of turns	N_{TX}, N_{RX}	16, 6	6, 6
Gap	d_1, d_2	5 mm	10 mm
Distance	h	150 mm	60 mm

method, we compare the PTE values derived from the calculated mutual inductance with the PTE values obtained from the S-parameter measurements. For comparison, two cases are considered: Case 1 is EV WPT and the resonance frequency of the coil is set to 85 kHz of SAE-J2954 standard [21]. Case 2 is the ISM (Industry Science Medical) band WPT, and the resonant frequency of the coil is 6.78 MHz. The experimental parameters for Case 1 and 2 are summarized in Table 1. Fig. 9 shows a measurement set-up in case 1 considering the coils suggested in [21]. Fig. 10 shows implemented Tx and Rx coils for the Case 2. S_{21} are measured using the Keysight P5004A vector network analyzer (VNA) in Case 1 and Agilent N9923A VNA in Case 2. The capacitance values used in the experiments are slightly different from the theoretically extracted values using $\omega_0 = 1/\sqrt{L_{TX}C_1} = 1/\sqrt{L_{RX}C_2}$. They are adjusted to achieve resonance at the given frequency considering parasitic reactance effects of the coils and the capacitors.

For both cases, the PTE curves versus position Δy (with

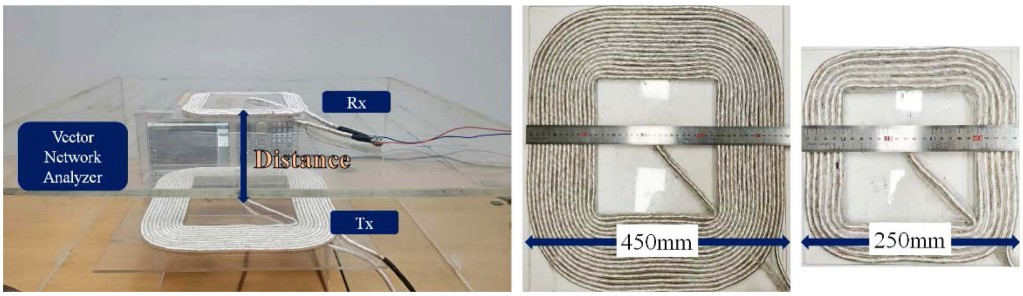

Fig. 9. (Color online) Measurement set-up for Case 1 (85 kHz WPT system).

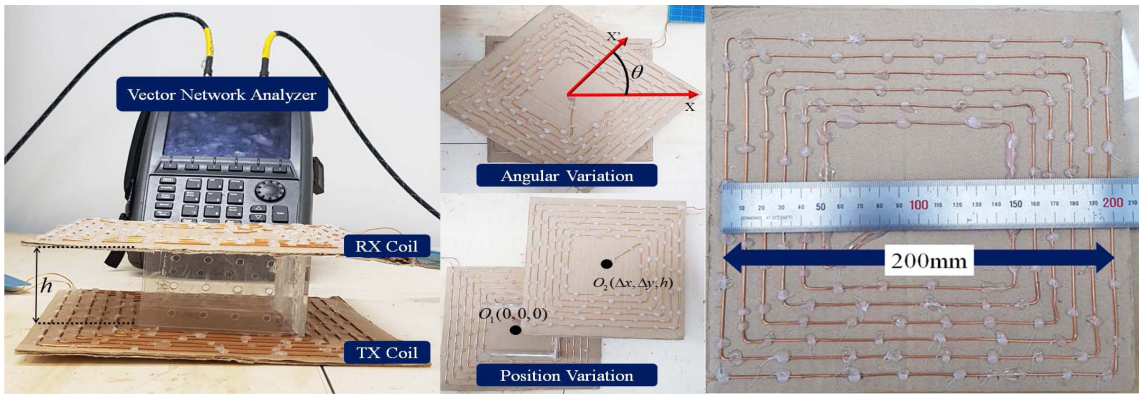

Fig. 10. (Color online) Measurement set-up for Case 2 (6.78 MHz WPT system).

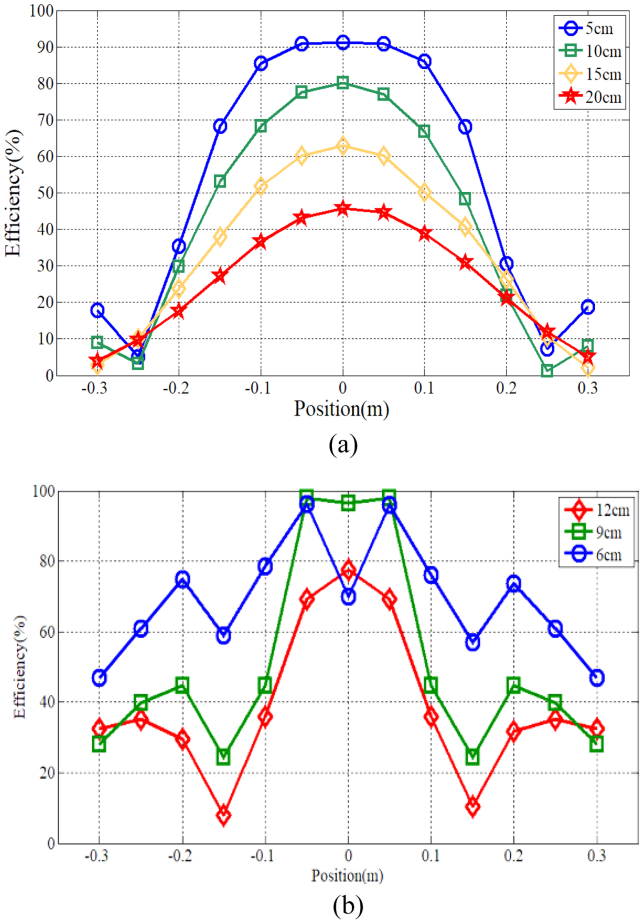

Fig. 11. (Color online) Measured result with various distance between Tx and Rr. (a) Case 1, (b) Case 2.

$\Delta x = 0$) by changing h are plotted in Fig. 11(a) and (b). As shown in Fig. 11(a), the PTE value at the aligned position decreases as h increases from 50 mm to 200 mm for the implemented 85 kHz system. However, in Fig. 11(b), the PTE value at the aligned position with h = 60 mm is lower than that with h = 90 mm, because over-coupling occurs at the vertical distance between 60 mm and 90 mm in the 6.78 MHz system.

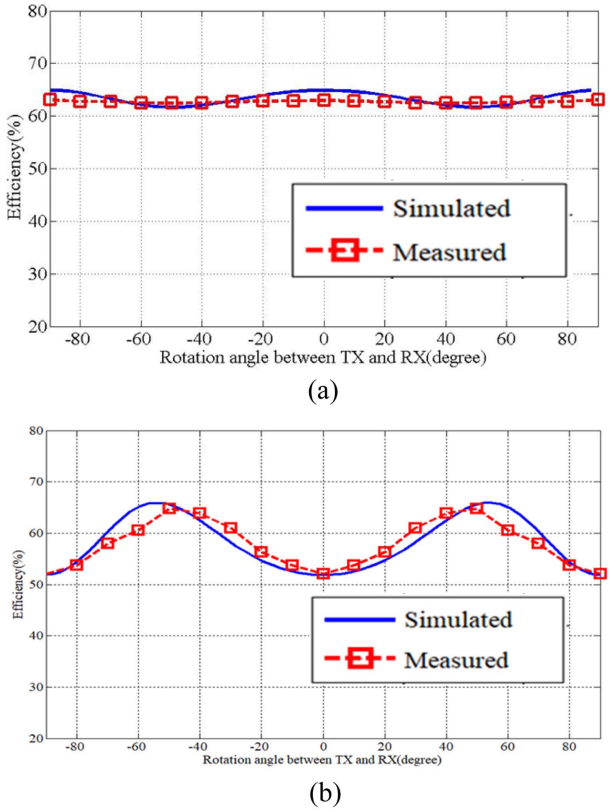

Fig. 12. (Color online) Simulated and measured PTE values for various rotated angles. (a) Case 1, (b) Case 2.

For a given vertical distance h (150 mm for Case 1 and 60 mm for Case 2) in Table 1, we simulate the PTE by changing the rotation angle of the Rx coil with respect to the z-axis. The predicted PTE using the calculated mutual inductance and the PTE of the WPT system derived from measured S-parameters by changing the rotation angles are plotted and compared in Fig. 12.

The predicted results are in good agreement with the

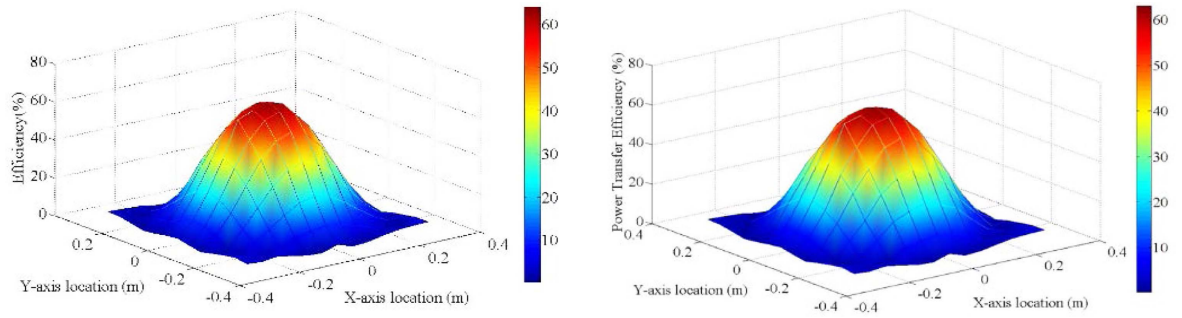

Fig. 13. (Color online) Simulated and measured PTE in Case 1 (distance = 0.15 m) with various horizontal positions of the Rx coil. (a) Simulated result, (b) Measured result.

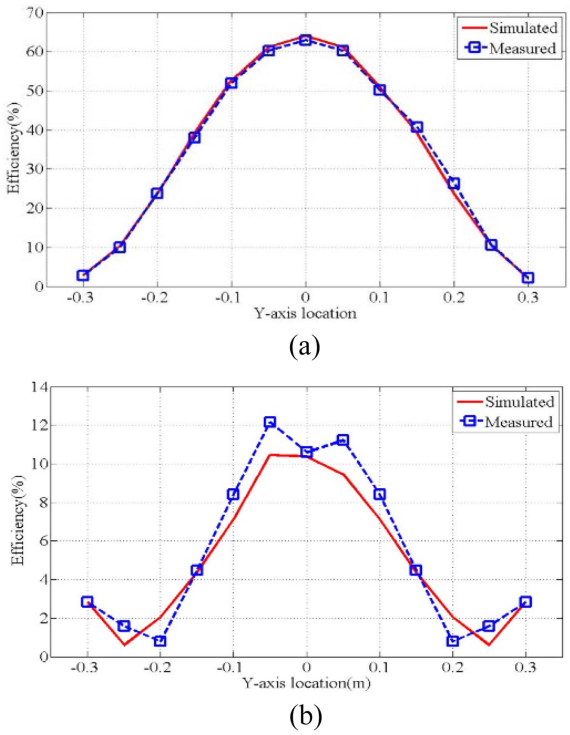

Fig. 14. (Color online) Simulated and measured PTE with Δy change in Case 1. (a) Δx = 0 m, (b) Δx = 0.25 m.

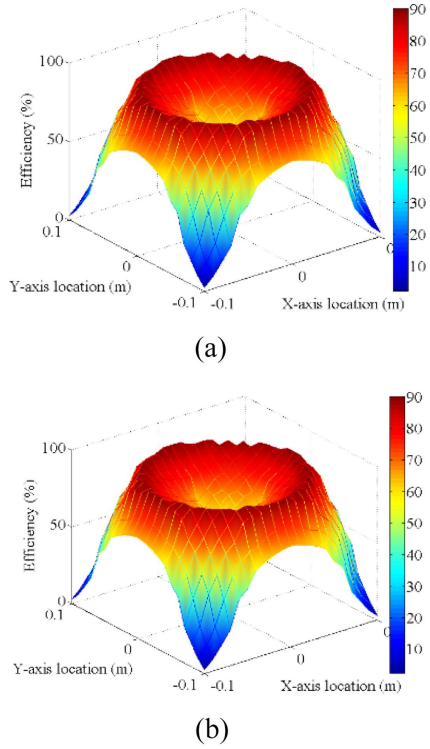

Fig. 15. (Color online) Simulated and measured PTE with various horizontal position of the Rx coil. (a) Simulated result, (b) Measured result.

measured results. In Fig. 12(a), the change in efficiency with respect to the angle change is smaller than that in Fig. 12(b) because the size of the Rx coil is smaller than the size of the Tx coil and the distance h is larger in Case 1. As shown in Fig. 12(b), the actual measured PTE value becomes maximum near the rotation angle value where the maximum PTE is expected to occur.

Figure 13(a) and (b) shows the simulated results and experimental results of the PTE obtained by changing the horizontal position of the Rx coil for Case 1. In this case, the predicted results are in good agreement with the measured results as well.

When the Rx coil is located coaxially with the Tx coil, the mutual inductance is maximum. It decreases as the horizontal distance between Tx and Rx coils increases. For the given h, the PTE is maximum at the aligned position and the PTE decreases as the horizontal distance from the aligned position increases.

Figure 14 is a graph comparing the simulation results with the measured results according to the position Δy change for the Δx = 0 m and 0.25 m for the Case 1. The solid line is the result of simulation, and the dotted line is the result of measurement.

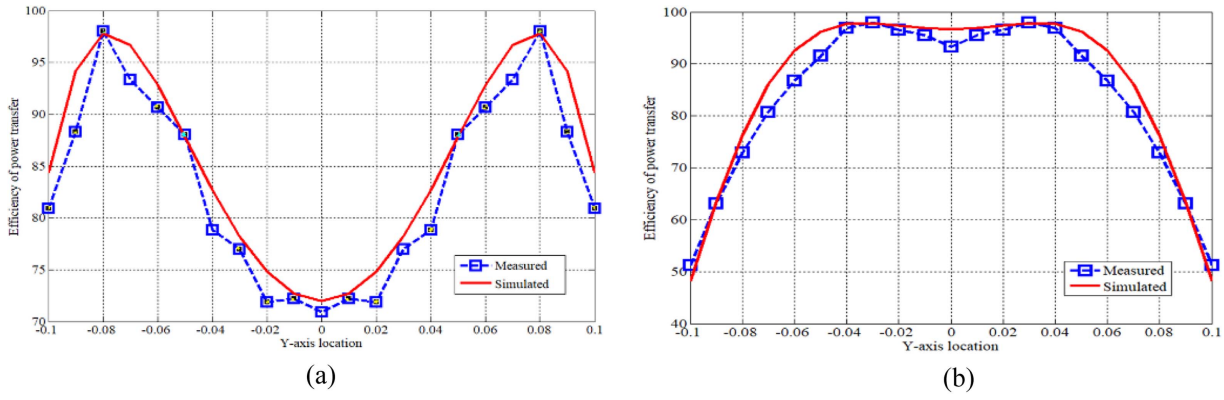

Fig. 16. (Color online) Simulated and measured PTE with Δy change in Case 2. (a) Δx = 0 m, (b) Δx = 0.07 m.

Table 2. NRMSE of the WPT system in Case 1 and Case 2.

NRMSE (%)	Case 1	Case 2
Angular Variation	1.88 %	3.74 %
Position Variation	5.82 %	5.49 %

Figure 15(a) and (b) shows the simulated results and experimental results of the PTE obtained by changing the horizontal position of the Rx coil for the Case 2. In this case, the predicted results are in good agreement with the measured results as well.

For the given h, the over-coupling between Tx and Rx occurs at the aligned position. Thus, the simulated and experimental results show that the locus of the maximum PTE values formed a circle with a center located at (0,0) in this case. It is possible to widen the range of the position of the Rx coil that maintains efficiency higher than a certain level in wireless charging using the over-coupling for the aligned Rx coil as shown in Fig. 15. Fig. 16 is a graph comparing the simulation results with the measured results to the position Δy change for the $\Delta x = 0$ m and 0.07 m.

In order to verify the similarity between the results from the proposed method and the experimental results, we calculate the normalized root mean square error (NRMSE) rate. Normalized RMSE is the RMSE value between the simulated and measured data divided by the average of the measured data. Table 2 shows NRMSE for Case 1 and Case 2.

6. Conclusions

In this paper, we proposed an analytical method to obtain the mutual inductance between two rectangular spiral coils using the Neumann formula and superposition, which is extended to the cases of angle and position change between two coils. The PTE of the magnetic resonant WPT system including misalignment situation can be predicted from the mutual inductance obtained by the proposed method. The accuracy of the proposed method was verified by comparing the predicted PTE values from the analyzed mutual inductance with the PTE values extracted from the measured S-parameters. For experimental verification, 85 kHz and 6.78 MHz magnetic resonant WPT systems were implemented. The cases with the angle and position variations of Rx coil for both two WPT systems were studied. For both cases, the results agree well with each other, and the accuracy of the proposed method can be confirmed by the NRMSE. The proposed mutual inductance calculation method can be applied to the coil design and simulation of WPT system.

Acknowledgements

This work was supported by the National Research Foundation of Korea (NRF) grant funded by the Korean government (MSIT) (NRF-2017R1A5A1015596), the Korea Institute for Advancement of Technology (KIAT) grant (HRD Program for Software-SoC convergence) (No. N0001883), and the Human Resource Program (Grant No. 20194010201790) of the Korea Institute of Energy Technology Evaluation and Planning (KETEP) grant funded by Korean government (MOTIE: the Ministry of Trade, Industry & Energy).

References

[1] C. Park, S. Lee, G. Cho, S. Choi, and C. Rim, IEEE Trans. Ind. App. **50**, 558 (2014).
[2] U. M. Jow and M. Ghovanloo, IEEE Trans. Bio. Sys. **1**, 193 (2007).
[3] E. Abdelhamid, K. AbdelSalam, A. Massoud, and S. Ahmed, IEEE ISIE, 10.1109/ISIE.2014.6864856 (2014).
[4] T. Campi, S. Cruciani, and M. Feliziani, Energies **11**, 352 (2018).
[5] J. Zhou, B. Zhang, W. Xiao, D. Qiu, and Y. Chen, IEEE Trans. Ind. Elec. **66**, 4097 (2019).
[6] S. H. Lee, K. P. Yi, and M. Y. Kim, Energies **12**, 371 (2019).
[7] J. Arteaga, S. Aldhaher, G. Kkelis, C. Kwan, D. C. Yates, and P. D. Mitcheson, IEEE Trans. Pow. Elec. **34**, 5093 (2019).
[8] W. Han, K. Chau, C. Jiang, W. Liu, and W. Lam, IEEE Trans. Mag. **55**, 7 (2019).
[9] E. Leuerer and W. Mokwa, Sensors **116**, 410 (2004).
[10] Y. Cheng, and Y. Shu, IEEE Trans. Mag. **50**, 1 (2014).
[11] W. Huang and H. Ku, J. E. Elec. Eng. **18**, 13 (2018).
[12] C. Yuhua and S. Yaming, IEEE Trans. Mag. **50**, 4 (2014).
[13] D. Wu, Q. Sun, X. Wang, and F. Yang, IET Pow. Elec. **11**, 781 (2018).
[14] R. Ditchburn and S. Burke, NDT & E Int. **38**, 690 (2005).
[15] H. Greenhouse, IEEE Trans. Parts. Hybrids and Pack. **10**, 101 (1974).
[16] J. Nadakuduti, M. Douglas, L. Lu, A. Christ, P. Guckian, and N. Kuster, IEEE Trans. Power Elec. **30**, 6264 (2015)
[17] T. Imura and Y. Hori, IEEE Trans. Ind. Elec. **58**, 4746 (2011).
[18] E. Simon-Tov, V. Tseng, S. Bedair, and N. Lazarus, IEEE Trans. Microwave Theory **66**, 5021 (2018).
[19] T. Imura, H. Okabe, and Y. Hori, IEEE VPPC, 10.1109/VPPC.2009.5289747 (2009).
[20] D. Frickey, IEEE Trans. Microwave Theory and Tech. **42**, 205 (1994).
[21] Z. Wei, W. Jeff, A. Arpith, and M. Chunting, IEEE Trans. Power Elec. **30**, 6356 (2015).